## EDGE ARTICLE

# Deep in blue with green chemistry: influence of solvent and chain length on the behaviour of *N*- and *N,N'*- alkyl indigo derivatives†

Daniela Pinheiro, [iD] [a] Marta Pineiro, [iD] [a] Adelino M. Galvão[b] and J. Sérgio Seixas de Melo [iD] *[a]

Using green chemistry procedures the synthesis of *N*-alkyl (NC$_n$Ind) and *N,N'*-dialkyl (N,N'C$_n$Ind) indigo derivatives, with $n$ = 1–3, 6, 8, 12 and 18, was undertaken, leading to compounds with blueish to greenish colors in solution. The effect of the alkyl chain length on the spectral (including color) and photophysical properties of the compounds was explored. This was done with solvents of different viscosities and polarities (dielectric constants). From time-resolved fluorescence and femtosecond-transient absorption (fs-TA) for the NC$_n$Ind derivatives with $n$ = 1 and 2, the decays are, in methylcyclohexane (MCH) and $n$-dodecane, single-exponential, while in 2-methyltetrahydrofuran (2MeTHF) they are bi-exponential. The excited state proton transfer (ESPT) is ultrafast (<1 ps) for NC$_{1,2}$Ind in MCH and $n$-dodecane, supported by time-dependent density functional theory (TDDFT) calculations, thus showing that both the chain length and solvent influence the ESPT process. For N,N'C$_n$Ind, from time-resolved experiments, and with the exception of the shortest member of the series, N,N'C$_1$Ind, two conformers are found to be present in the excited state.

## Introduction

Indigo has been rightfully considered an iconic dye used from ancient times till today when it remains popular and is used worldwide for dyeing denim.[1] Indigo can be extracted from plants (more than 700 different *Indigofera* species are found in nature)[2] or industrially synthesized. In this last case it is linked to the modern chemical industry and the rise of the industrial revolution that led to a reconsideration of the use of natural supplies.[1–3]

The longevity of indigo usage is chemically related to its (photo)stability which is linked to the highly efficient internal conversion and inefficient intersystem crossing and fluorescence.[2,3] The highly efficient deactivation process of the excited state of indigo has been associated with a mechanistic process resulting from a fast excited state proton transfer (ESPT) between a carbonyl group and the adjacent nitrogen proton.[2,4–9] In the ground state, indigo remains in a stable trans-planar configuration, as a result of the hydrogen bond originating from the two C=O and two N–H groups, thus preventing *trans*–

*cis* photochemical isomerization.[2,10,11] Yet, structural changes in indigo may tune its photochemical and photophysical properties. The more common modification consists in the replacement of hydrogen atoms at the 4-, 5-, 6- and 7-position of the phenyl ring with other atoms, or groups of atoms, *e.g.*, methyl, halogen, methoxy groups.[9,12,13] Replacement of both hydrogen atoms of the N–H groups in indigo by different groups has also been described and unexpected properties were observed.[14–20] Indigo derivatives, which are not secondary amines and cannot establish intramolecular hydrogen bonds, showed photoinduced isomerizations.[10,11,21–24] *Trans–cis* isomerization of *N,N'*-substituted indigo derivatives has been studied since at least 1968 with the work of Giuliano *et al.* where reversible photoisomerizations were reported for *N,N'*-dimethylindigo in benzene.[25]
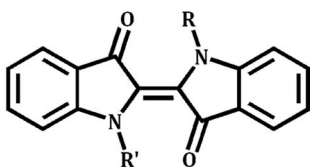
In the present work, modifications of the chromophoric core (H-chromophore) of indigo, following a similar methodology to that reported by Setsune,[26] were undertaken by replacing one or two hydrogens of indigo's N–H groups with alkyl groups with an increased number of carbons (see Scheme 1). A total of seven *N*-alkyl indigo derivatives and seven *N,N'*-dialkyl indigo derivatives have been synthesized and investigated in different solvent media in order to study the influence of the substitution of the alkyl groups on the electronic spectral, photophysical and photochemical properties of the compounds. The observed properties and behaviour were further rationalized with the help of TDDFT computational studies.

*[a]University of Coimbra, CQC, Department of Chemistry, Rua Larga, 3004-535 Coimbra, Portugal. E-mail: sseixas@ci.uc.pt*

*[b]Centro de Química Estrutural, Departamento de Engenharia Química, Instituto Superior Técnico (IST), Universidade de Lisboa, Av. Rovisco Pais, 1049-001 Lisboa, Portugal*

Scheme 1 Structures and acronyms of indigo, and N- and N,N'-alkyl indigo derivatives.

| Compound | Substituent | Acronym |
|----------|-------------|---------|
| **Indigo** | R,R'=H | Ind |
| ***N*-alkyl Indigo Derivatives** | | NC$_n$Ind |
| *N*-methylindigo | R=CH$_3$; R'=H | NC$_1$Ind |
| *N*-ethylindigo | R=C$_2$H$_5$; R'=H | NC$_2$Ind |
| *N*-propylindigo | R=C$_3$H$_7$; R'=H | NC$_3$Ind |
| *N*-hexylindigo | R=C$_6$H$_{13}$; R'=H | NC$_6$Ind |
| *N*-octylindigo | R=C$_8$H$_{17}$; R'=H | NC$_8$Ind |
| *N*-dodecylindigo | R=C$_{12}$H$_{25}$; R'=H | NC$_{12}$Ind |
| *N*-octadodecylindigo | R=C$_{18}$H$_{37}$; R'=H | NC$_{18}$Ind |
| ***N,N'*-dialkyl Indigo Derivatives** | | N,N'C$_n$Ind |
| *N,N'*-dimethylindigo | R,R'=CH$_3$ | N,N'C$_1$Ind |
| *N,N'*-diethylindigo | R,R'=C$_2$H$_5$ | N,N'C$_2$Ind |
| *N,N'*-dipropylindigo | R,R'=C$_3$H$_7$ | N,N'C$_3$Ind |
| *N,N'*-dihexylindigo | R,R'=C$_6$H$_{13}$ | N,N'C$_6$Ind |
| *N,N'*-dioctylindigo | R,R'=C$_8$H$_{17}$ | N,N'C$_8$Ind |
| *N,N'*-didodecylindigo | R,R'=C$_{12}$H$_{25}$ | N,N'C$_{12}$Ind |
| *N,N'*-dioctadodecylindigo | R,R'=C$_{18}$H$_{37}$ | N,N'C$_{18}$Ind |

# Results and discussion

### Synthesis of the *N*- and *N,N'*-alkyl indigo derivatives

The synthesis of *N*- and *N,N'*-alkyl indigo derivatives was performed by using a typical substitution reaction of iodoalkanes using sodium hydride (NaH) as a base and *N*-dimethylformamide (DMF) as a solvent.[26,27] The reaction was performed under microwave (MW) irradiation and the overall reaction pathway is illustrated in Scheme 2. Under MW irradiation conditions, the amount of solvent necessary to perform the reaction is strongly reduced and the reaction time decreased when compared to conventional reaction procedures.[14]

### General synthetic procedure

In a thick-glass microwave reactor, with a magnetic stirring bar, indigo (1 equiv.) and NaH (2 equiv.) were dissolved in 1 mL DMF. The corresponding alkyl halide (R–I) was added (4 equiv.)



R,R'= CH$_3$, C$_2$H$_5$, C$_3$H$_7$, C$_6$H$_{13}$, C$_8$H$_{17}$, C$_{12}$H$_{25}$, C$_{18}$H$_{37}$
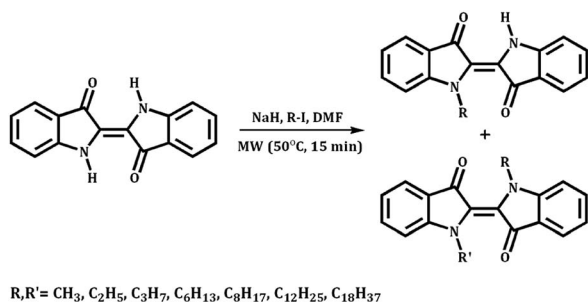
Scheme 2 General synthetic procedure followed for the synthesized indigo derivatives.

and solvent was added to a total volume of 2 mL. The resulting mixture was heated under microwave irradiation at 50 °C for 15 minutes.

After cooling down to room temperature, the reaction mixture was extracted with dichloromethane and water and the organic layer was dried overnight with anhydrous sodium sulfate. After this, the mixture was filtered and the solvent concentrated under reduced pressure.

The crude was purified by column chromatography (SiO$_2$) using dichloromethane as an eluent to give *N*- and *N,N'*-alkyl indigo derivatives, as blue and green powders, respectively.

These reactions provide both mono- and di-substituted indigos from the abundant and inexpensive parent compound indigo in a straightforward manner. In contrast to their parent indigo precursor, all compounds are readily soluble in most organic solvents, simplifying the purification, characterization and further processing.

The molecular structures of all the *N*- and *N,N'*-alkyl indigo derivatives were confirmed by ${}^1$H and ${}^{13}$C nuclear magnetic resonance (NMR) spectroscopy and further by gas chromatography-mass spectrometry (GC-MS) and/or high resolution mass spectrometry (HRMS). The obtained data were in accordance with the structure proposed. Detailed information on the ${}^1$H and ${}^{13}$C NMR spectroscopy, GC-MS and/or HRMS characterization is given in the ESI.†

### Ground and excited state characterization

**Absorption and steady state fluorescence spectral data.** The absorption and fluorescence spectra of indigo, and *N*-alkyl and *N,N'*-dialkyl indigo derivatives were obtained in seven solvents with different dielectric constants ($\varepsilon$) and viscosities ($\eta$) at room temperature ($T = 293$ K). In Fig. 1 a picture of the solution colors of the *N*- and *N,N'*-alkyl indigo derivatives in *n*-dodecane is shown. It can be seen that for the *N*-alkyl mono-substituted derivatives the color is close to that of the blue indigo (wavelength maximum, $\lambda_{max}^{abs}$, of 602 nm in 2-methyltetrahydrofuran, 2MeTHF) with $\lambda_{max}^{abs}$ ranging from 622 nm to 632 nm, while for the di-substituted derivatives the shortest member of the series, N,N'C$_1$Ind, displays a $\lambda_{max}^{abs}$ different from that of all the other N,N'C$_n$Ind derivatives.

Fig. 1 also shows the absorption and emission spectra of indigo, and *N*- and *N,N'*-alkyl indigo derivatives investigated in 2MeTHF and dimethylsulfoxide (DMSO) at $T = 293$ K. A more careful observation of this figure shows that (i) the absorption and emission of indigo are blue-shifted relative to all other indigo derivatives; (ii) the full width at half maximum (FWHM) values of the absorption spectra of indigo and the *N,N'*-dialkyl indigo derivatives are similar (FWHM = 1515 cm$^{-1}$) while *N*-alkyl indigo derivatives present a higher value (FWHM = 2129 cm$^{-1}$); however (iii), the same does not occur with the emission spectra where now it is indigo and the *N,N'*-dialkyl indigo derivatives that display similar (and lower) FWHM values relative to the *N*-alkyl indigo derivatives. The overall data seem to indicate that there are different contributions to the ground and excited state geometries of the *N*- and *N,N'*-alkyl indigo derivatives. In the case of the *N*-alkyl indigo derivatives the
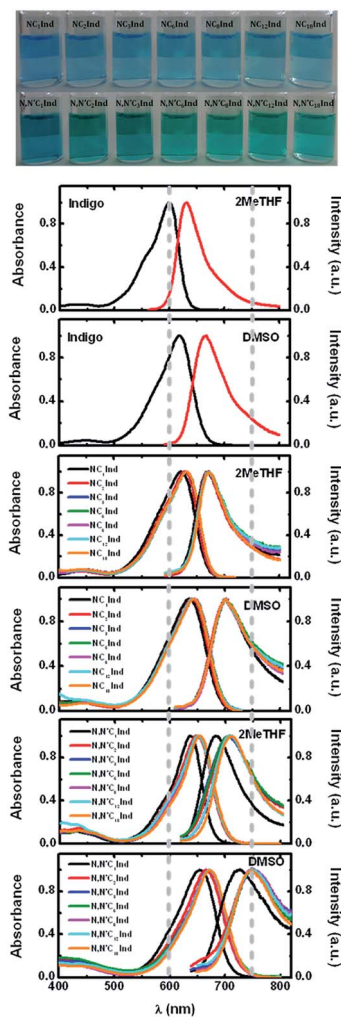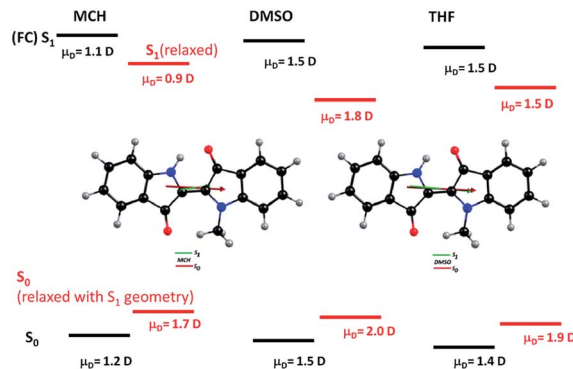
Fig. 1 (Top) Picture of *N*- and *N,N*′-alkyl indigo derivatives in *n*-dodecane at *T* = 293 K. (Bottom) Normalized absorption and fluorescence emission spectra of *N*- and *N,N*′-alkyl indigo derivatives in 2MeTHF and DMSO solutions at *T* = 293 K. For indigo the same parameters are also presented for comparison. The dashed vertical lines are meant to be a guide to the eye in the red-shift from indigo to NC$_n$Ind and N,N′C$_n$Ind.



Scheme 3 Schematic representations of the dipole moments of the ground state (S$_0$), excited singlet state (Franck–Condon state, FC) and in the relaxed geometry (after solvent reorientation), S$_1$ relaxed, and of the ground state with S$_1$ geometry (S$_0$ relaxed with S$_1$ geometry) for NC$_1$Ind in MCH, DMSO and THF. The inset in the middle shows dipole moments of the ground state and excited state for the adiabatically relaxed structures in the emission geometry.

square of the refractive index, which can be roughly considered to be the same in all solvents), in emission, relaxation to the adiabatic surface has already occurred making it much more sensitive to, and strongly influenced by, the value of the dipole moment (Scheme 3).

Using the shortest member of the series, NC$_1$Ind, as an illustrative example, Scheme 3 shows how the solvent influences the polarization of the ground and singlet excited states (relaxed structures in the S$_0$ – relaxed with S$_1$ geometry – and S$_1$ potential energy surfaces (PESs), S$_1$ relaxed), the effect being more marked in the emission. The charge redistribution due to excitation/de-excitation is more marked in the emission geometry. Indeed, by changing from a non-polar solvent (MCH) to

narrower band spectra mirror the fact that there is a single geometry in the ground state (and singlet excited state), while for the *N,N*′-dialkyl indigo derivatives the more broad nature of the absorption and emission spectra suggests that in the solvents MCH and *n*-dodecane it is likely that more than one conformer in the ground and excited states exists. These interpretations will be further addressed and fully justified from TDDFT calculations.

The spectral properties (absorption and fluorescence emission) show that while there is little dependence of the absorption on solvent polarity (relatively small red-shift), there is a pronounced red-shift of the emission spectra, which is also mirrored by a high Stokes shift ($\Delta_{SS}$, see Fig. SI1 and SI2†).

TDDFT calculations show that while in absorption, excitation is to the Franck–Condon (FC) S$_1$ surface, and only dependent on the fast component of polarization (quantified by the

Table 1 Spectroscopic properties, including wavelength maxima for absorption ($\lambda_{Abs}$) and fluorescence ($\lambda_{Fluo}$) and Stokes shift ($\Delta_{SS}$) for the *N*-alkyl indigo derivatives in 2MeTHF and DMSO solutions at *T* = 293 K. For indigo (Ind) the same parameters are also presented for comparison. The solvent properties (viscosity, $\eta$, in cP and dielectric constant $\varepsilon$) are also given

| Compound | Solvent | $\eta$ (cP) | $\varepsilon$ | $\lambda_{Abs}$ (nm) | $\lambda_{Fluo}$ (nm) | $\Delta_{SS}$ (cm$^{-1}$) |
|---|---|---|---|---|---|---|
| **Ind** | **2MeTHF** | 0.575 | 7.58 | 602 | 631 | 763 |
| | **DMSO** | 1.991 | 46.45 | 619 | 665 | 1117 |
| **NC$_1$Ind** | **2MeTHF** | 0.575 | 7.58 | 622 | 670 | 1152 |
| | **DMSO** | 1.991 | 46.45 | 635 | 700 | 1462 |
| **NC$_2$Ind** | **2MeTHF** | 0.575 | 7.58 | 629 | 671 | 995 |
| | **DMSO** | 1.991 | 46.45 | 641 | 700 | 1315 |
| **NC$_3$Ind** | **2MeTHF** | 0.575 | 7.58 | 631 | 671 | 945 |
| | **DMSO** | 1.991 | 46.45 | 644 | 700 | 1242 |
| **NC$_6$Ind** | **2MeTHF** | 0.575 | 7.58 | 632 | 672 | 942 |
| | **DMSO** | 1.991 | 46.45 | 644 | 702 | 1283 |
| **NC$_8$Ind** | **2MeTHF** | 0.575 | 7.58 | 632 | 673 | 964 |
| | **DMSO** | 1.991 | 46.45 | 644 | 702 | 1283 |
| **NC$_{12}$Ind** | **2MeTHF** | 0.575 | 7.58 | 632 | 673 | 964 |
| | **DMSO** | 1.991 | 46.45 | 644 | 703 | 1303 |
| **NC$_{18}$Ind** | **2MeTHF** | 0.575 | 7.58 | 632 | 673 | 964 |
| | **DMSO** | 1.991 | 46.45 | 644 | 704 | 1323 |

a polar one (DMSO), the difference in the ground state dipole in the $S_1$ geometry ($\Delta_{MCH-DMSO}$, $S_0$ with relaxed $S_1$ geometry) increases by 18% (from 1.7 D to 2.0 D) but doubles (100% increase) in the $S_1$ relaxed excited state ($\Delta_{MCH-DMSO}$, $S_1$ relaxed) from 0.9 D in MCH to 1.8 D in DMSO (see Table SI1 and Fig. SI3 in the ESI†).

This can be further complemented with TDDFT calculations of Franck–Condon (FC) state excitations, in $S_1$ emission geometries, whose difference from the adiabatic surface constitutes a qualitative measurement of the contribution of the dipole solvent stabilization to the Stokes shift. This ranges from 0 cm$^{-1}$ (in MCH) to 1024 cm$^{-1}$ (in DMSO), with an intermediary value of 758 cm$^{-1}$ (in tetrahydrofuran (THF)).

Tables 1 and 2 summarize the spectral data for N- and N,N'-alkyl indigo derivatives and of indigo in 2MeTHF and DMSO. Full data details in all solvents are available in Tables SI2 and SI3 in the ESI.†

From Table 1 and Fig. 2, it can be seen that although the $\lambda_{max}^{abs}$ of NC$_1$Ind and NC$_2$Ind displays a small blue-shift when compared to the other N-alkyl indigo derivatives, the fluorescence emission maxima (and spectra) are essentially identical, despite the increase in the size of the alkyl chain (from NC$_3$Ind to NC$_{18}$Ind). Similar behaviour was also observed with the N,N'-dialkyl indigo derivatives. Indeed, these display lower values for the absorption wavelength maxima of N,N'C$_1$Ind when compared with the remaining N,N'-dialkyl indigo derivatives (Table 2 and Fig. 2). However, contrasting with the behaviour observed for the N-alkyl indigo derivatives, the fluorescence emission band of N,N'C$_1$Ind is blue-shifted (~20–30 nm) relative to that observed for the other N,N'-dialkyl derivatives (N,N'C$_2$Ind to N,N'C$_{18}$Ind, see Fig. 1).

### Photophysical properties in solution

**Fluorescence quantum yields.** The fluorescence quantum yield values obtained at $T = 293$ K for the N-alkyl and N,N'-
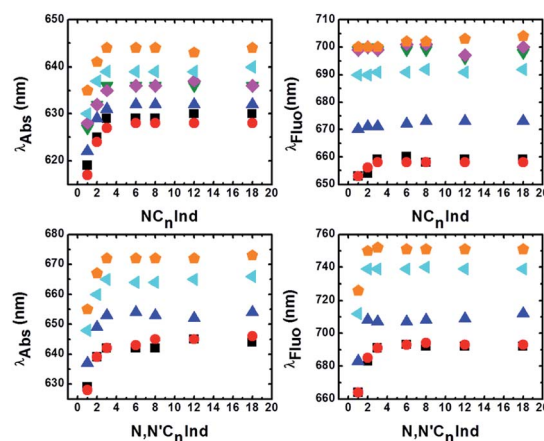


**Fig. 2** Dependence of the spectroscopic properties (wavelength maxima of absorption, $\lambda_{Abs}$, and of fluorescence, $\lambda_{Fluo}$) for the N-alkyl (NC$_n$Ind) and N,N'-dialkyl (N,N'C$_n$Ind) indigo derivatives on n-dodecane (black squares), MCH (red circles), 2MeTHF (blue triangles), EtOH (green triangles), MeOH (pink rhombi), DMF (cyan triangles) and DMSO (orange pentagons) at $T = 293$ K.

dialkyl indigo derivatives and indigo in solvents of different polarities (ranging from the non-polar n-dodecane and MCH, to the more polar DMSO and DMF, as indicated by the dielectric constant value, $\varepsilon$) are depicted in Fig. 3.

From Fig. 3 (and Table SI4†) four main observations can be made. The first (i) is that the fluorescence quantum yields of the N-alkyl indigo derivatives are much lower than those of indigo (ca. 3-fold lower in DMF). The second (ii) observation results from the fact that for the N-alkyl indigo derivatives the fluorescence quantum yields are basically identical in 2MeTHF,
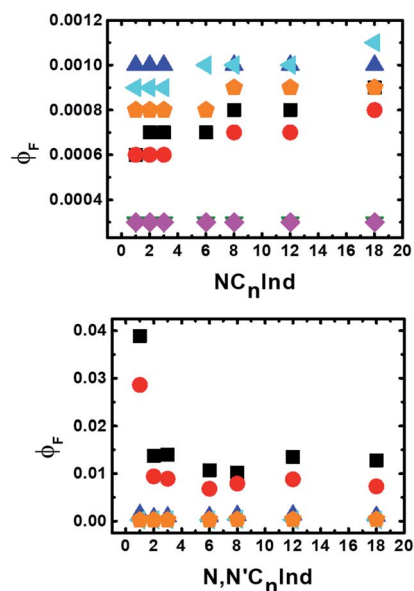
**Table 2** Spectroscopic properties, including wavelength maxima for absorption ($\lambda_{Abs}$) and fluorescence ($\lambda_{Fluo}$) and Stokes shift ($\Delta_{SS}$) for the N,N'-dialkyl indigo derivatives in 2MeTHF and DMSO solutions at $T = 293$ K. The solvent properties (viscosity $\eta$ in cP and dielectric constant $\varepsilon$) are also given

| Compound | Solvent | $\eta$ (cP) | $\varepsilon$ | $\lambda_{Abs}$ (nm) | $\lambda_{Fluo}$ (nm) | $\Delta_{SS}$ (cm$^{-1}$) |
|---|---|---|---|---|---|---|
| N,N'C$_1$Ind | 2MeTHF | 0.575 | 7.58 | 637 | 683 | 1057 |
| | DMSO | 1.991 | 46.45 | 655 | 726 | 1493 |
| N,N'C$_2$Ind | 2MeTHF | 0.575 | 7.58 | 649 | 708 | 1284 |
| | DMSO | 1.991 | 46.45 | 667 | 750 | 1650 |
| N,N'C$_3$Ind | 2MeTHF | 0.575 | 7.58 | 653 | 707 | 1170 |
| | DMSO | 1.991 | 46.45 | 672 | 752 | 1583 |
| N,N'C$_6$Ind | 2MeTHF | 0.575 | 7.58 | 654 | 707 | 1146 |
| | DMSO | 1.991 | 46.45 | 672 | 751 | 1565 |
| N,N'C$_8$Ind | 2MeTHF | 0.575 | 7.58 | 653 | 708 | 1190 |
| | DMSO | 1.991 | 46.45 | 672 | 751 | 1565 |
| N,N'C$_{12}$Ind | 2MeTHF | 0.575 | 7.58 | 652 | 708 | 1233 |
| | DMSO | 1.991 | 46.45 | 672 | 751 | 1565 |
| N,N'C$_{18}$Ind | 2MeTHF | 0.575 | 7.58 | 654 | 712 | 1246 |
| | DMSO | 1.991 | 46.45 | 673 | 751 | 1543 |



**Fig. 3** Variation of the fluorescence quantum yields ($\phi_F$) for the N-alkyl (NCnInd) and N,N'-dialkyl (N,N'CnInd) indigo derivatives in n-dodecane (black squares), MCH (red circles), 2MeTHF (blue triangles), EtOH (green triangles), MeOH (pink rhombi), DMF (cyan triangles) and DMSO (orange pentagons) at $T = 293$ K.

ethanol (EtOH) and methanol (MeOH) and close (in values) in the other solvents despite the increase of the alkyl chain length. For the $N,N'$-dialkyl indigo derivatives it is seen that (iii), with the exception of N,N'C$_1$Ind in $n$-dodecane and MCH (which display higher $\phi_F$ values), the quantum yield values remain approximately identical in 2MeTHF, DMF and DMSO despite the increase of the alkyl chain length (see Table SI5†). Finally (iv), a comparison of the $\phi_F$ values for the mono- and di-substituted indigo derivatives shows that the latter ($N,N'$-dialkyl indigo derivatives) have higher values in $n$-dodecane and MCH. This shows that in these solvents and for N,N'C$_1$Ind and N,N'C$_2$Ind, the radiative deactivation channel has a higher contribution than in the higher alkyl chain derivatives ($n \geq 3$).

**Rates of the excited state deactivation pathways.** From the $\phi_F$ and the longer component, $\tau_2$, of the bi-exponential fluorescence decays (see the next section), the radiative ($k_F$) and radiationless ($k_{NR}$) rate constants for the different $N$- and $N,N'$-alkyl indigo derivatives could be obtained (see Tables SI4 and SI5 in the ESI†).

For the $N$-alkyl indigo derivatives the $k_F$ values are approximately $1$–$2 \times 10^{-2}$ ns$^{-1}$ while the $k_{NR}$ values are 4 orders of magnitude higher (with indigo the $k_{NR}$ values are only 3 times higher than $k_F$), thus showing that, as with indigo, more than 99.9% of the quantum loss occurs through the radiationless internal conversion channel. Contrasting with this behaviour is the observation that for the $N,N'$-dialkyl indigo derivatives in non-polar solvents ($n$-dodecane and MCH) the $\phi_F$ values are $1$–$2$ orders of magnitude higher than those in polar solvents (DMF, DMSO and even 2MeTHF). This is also reflected in the $\tau_F$ values and consequently in the ratio of the radiationless ($k_{NR}$) and radiative ($k_F$) constants (see Tables SI4 and SI5†).

TDDFT calculations were used to probe S$_0$ and S$_1$ surfaces by rotation around the central C=C bond (atoms and bonds in white in Scheme 4). As illustrated in Scheme 4, in the ground state, rotation around the central C=C bond is precluded by an activation barrier of 103 kJ mol$^{-1}$. In contrast, in the excited state this barrier drops almost six-fold to 17.6 kJ mol$^{-1}$. Nevertheless just a few degrees after crossing the top of the barrier a sloped conical intersection (CI) deactivates non-radiatively to the ground state, rotating back to the *trans*
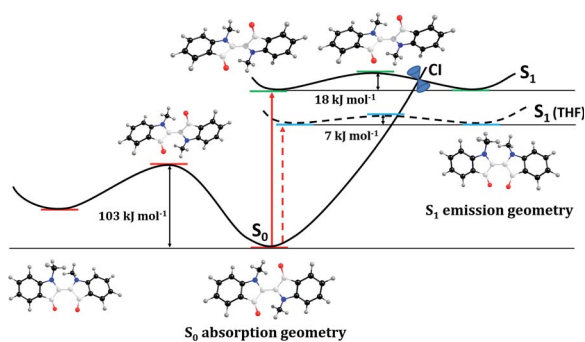


**Scheme 4** Gas phase probing of S$_0$ and S$_1$ surfaces by rotation around the central C=C bond (dihedral coordinate highlighted in white) for N,N'C$_1$Ind. The effect of solvent (THF) on the excited state S$_1$ activation energy barrier is also depicted (see text for more details).

structure, instead of proceeding with an additional rotation to achieve the *cis* structure. This mirrors the behaviour observed in non-polar solvents. As the solvent polarity increases, the process becomes progressively less activated (*e.g.* 7 kJ mol$^{-1}$ in THF), increasing the efficiency of this radiationless decay channel relative to the radiative channel with a corresponding drop in fluorescence quantum yield, lifetime and rate constant. This will be further complemented on the basis of the time resolved data in the next section.

## Molecular deactivation mechanisms from time-resolved experiments: picosecond (ps)-time-resolved fluorescence and femtosecond (fs)-transient absorption difference

### $N$-Alkyl indigo derivatives

*ps-time-resolved fluorescence.* In contrast to other systems, where two emissive species are clearly seen,[28–31] in the case of indigo the evidence for the presence of two excited state species is given from the bi-exponential nature of the time-resolved fluorescence measurements also observed with fs-transient difference absorption (fs-TA).[5,9,11,32] The two-state system in the excited state is consistent with a *keto*-excited form giving rise to the *enol* form of indigo by fast single proton transfer (SPT).[5,7,9,32] The presence of the rising component (negative pre-exponential value) at longer emission wavelengths (Table SI6†) is of particular relevance, demonstrating that the second species (the long-living *enol*) is formed at the expense of the short-living *keto* species.[8]

From the present data, with the exception of NC$_1$Ind and NC$_2$Ind in $n$-dodecane and MCH, all the other $N$-alkyl indigo derivatives could be well fitted with a bi-exponential decay law according to eqn (1) (with $n = 2$).

$$I(t) = \sum_{i,j=1}^{n} a_{ij} e^{-t/\tau_i} \qquad (1)$$

where $\tau_i$ are the decay times and $a_{ij}$ the pre-exponential factors which represent the contribution of each exponential term at $t = 0$.

In $n$-dodecane and MCH, the fluorescence decays of NC$_1$Ind and NC$_2$Ind could be well fitted with a single exponential decay law according to eqn (1) (with $n = 1$) (see Table SI6†), which, as will be discussed below, is due to the fast ESPT in these compounds found to be below 1 ps. It is also worth noting that in the studied solvents intermolecular excited proton transfer (to the solvent) is precluded, a mechanism that has been proposed to exist with indigo carmine.[33,34] However, inter-molecular (but involving two NC$_1$Ind molecules), *i.e.* dimeric, species are predicted from TDDFT (see the discussion at the end of this section), which may explain the very fast ESPT in these compounds. Fig. 4A and B (and detailed data in Table SI6†) show the fluorescence for NC$_1$Ind in MCH and 2MeTHF in addition to that for the long-chain NC$_{18}$Ind in MCH. The mono-exponential decay for NC$_1$Ind in MCH shows that only the *enol* form is able to be observed (with a value of 32.3 ps), while for NC$_1$Ind in 2MeTHF and NC$_{18}$Ind in MCH, the *keto* species (associated with the ESPT) is observed (10.8 ps for NC$_1$Ind; 9.8 ps for NC$_{18}$Ind) together with the decay of the *enol* (66.2 ps for
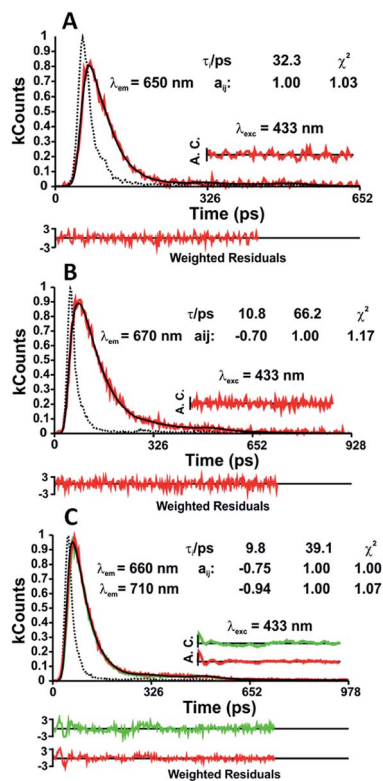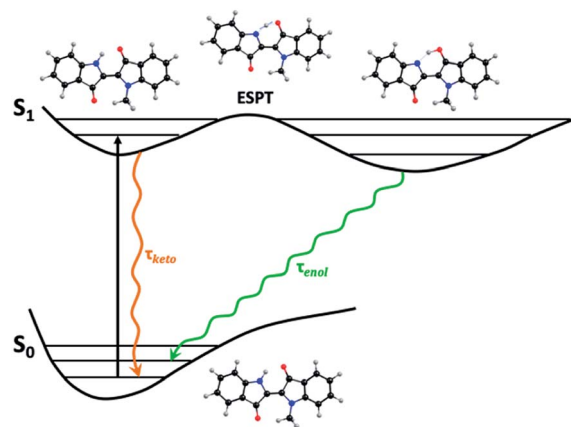
Fig. 4 Fluorescence decays of NC$_1$Ind in MCH (A) and 2MeTHF (B) and NC$_{18}$Ind in MCH (C) obtained at $T = 293$ K. The fluorescence decay times ($\tau_i$) and the associated pre-exponential factors ($a_{ij}$) are presented in the inset. For a better judgment of the quality of the fits, the weighted residuals, autocorrelation functions (ACs) and chi-squared ($\chi^2$) values are also shown. The dashed line in the decays is the pulse instrumental response.



Scheme 5 Schematic view of the *keto/enol* tautomerization occurring through an internal proton transfer. Saddle geometry depicting the 710 cm$^{-1}$ imaginary frequency mode.

Table 3 Bond distances and dihedral angles for NC$_1$Ind obtained from TDDFT calculations

| Bond distances (pm) and dihedral angles (°) | keto | Saddle point | enol |
|---|---|---|---|
| C=O (pm) | 123.1 | 128.6 | 131.4 |
| O–H (pm) | 187.0 | 120.7 | 101.7 |
| N–H (pm) | 101.4 | 128.3 | 163.1 |
| N–C–C–C (°) | 2.9 | 1.4 | 2.1 |
| O–C–C–C (°) | 0.5 | 0.8 | 0.7 |

NC$_1$Ind; 39 ps for NC$_{18}$Ind). If one considers an Arrhenius type behaviour and the activation barriers given by TDDFT calculations, with values of 3.0 kJ mol$^{-1}$ and 9.5 kJ mol$^{-1}$ in MCH and THF, respectively, one obtains a ratio of $k_{MCH}/k_{2MeTHF} = 14.4$. If now one uses the value of $k_{2MeTHF}$ as the value of $k_{ESPT} = 1/10.8$ ps $= 9.3 \times 10^{10}$ s$^{-1}$ in this solvent and assuming that $k_{MCH}/k_{2MeTHF}$ is 14.4, one obtains $k_{ESPT} = 1/0.75$ ps, leading to a value $(1.33 \times 10^{12}$ s$^{-1})$ that is beyond the time resolution and therefore not observed in the ps-TCSPC measurements and is likely to be mixed up with the solvent reorientation decay component in the fs-TA measurements.

In agreement with previous experimental and theoretical studies,[5] density functional theory (DFT) and TDDFT calculations predict a possible internal ESPT corresponding to a *keto/enol* tautomerization, Scheme 5, through the N–H stretching frequency which has a saddle point with an imaginary frequency of 710 cm$^{-1}$. This process, already reported previously,[5] although activated (3.0 kJ mol$^{-1}$ in MCH and 9.5 kJ mol$^{-1}$ in THF), is a spontaneous process if corrected to zero point vibrational (ZPV) energy (the N–H stretching mode, which becomes a translation mode at the saddle geometry, has a ZPV energy of 19 kJ mol$^{-1}$).

The relevant bond distances and dihedral angles in the ESPT in NC$_1$Ind (Table 3) pertaining to the change in the N–H and

C=O bonds in the *keto* and (*via* the saddle point) *enol* forms, and the fact that the system remains almost planar explains the fast ESPT ($k_{ESPT} = 1.33 \times 10^{12}$ s$^{-1}$) observed.

Moreover, after ESPT, rotation around the central C=C bond would provide access to a CI as a channel for deactivation to the ground state (Scheme 4). This mechanism is in fact observed for all systems in polar solvents as well as in NC$_n$Ind with alkyl chains longer than or equal to $n = 3$, failing for the two shortest chain compounds NC$_1$Ind and NC$_2$Ind. With the two shortest members of the series, DFT calculations are compatible with the existence of a dimeric species, as depicted in Scheme 6, which, in MCH, is stable by 40 kJ mol$^{-1}$ when compared with the two isolated monomers but unstable by 50 kJ mol$^{-1}$ in THF (the absolute values of stabilization energy should be taken cautiously because they may be hampered by basis set superposition errors). In the gas phase, the localized molecular orbital energy decomposition analysis was used for estimation of basis set superposition errors using the Boys and Bernardi counterpoise method.[35] The interaction energy drops from 52 to 33 kJ mol$^{-1}$. If these results are transposed to MCH (which is a non-polar solvent) by applying a similar scaling factor, the 40 kJ mol$^{-1}$ stabilization energy would drop to 25 kJ mol$^{-1}$.

The dimeric species may experimentally be pre-formed during the crystal dissolution process or by equilibration from monomers. This process is favorable in non-polar solvents when the polar groups are hidden from the non-polar solvent molecules.
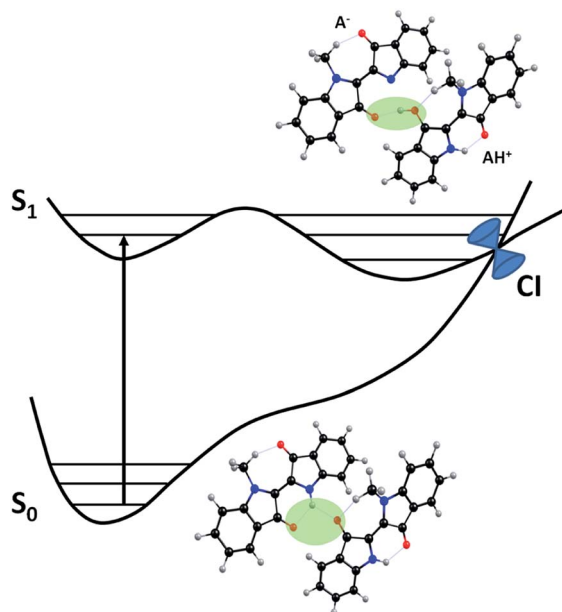
**Scheme 6** Schematic diagram with the dimeric species predicted for NC$_1$Ind by DFT calculations and the S$_1$ ESPT conjugated A$^-$/AH$^+$ pair. The reaction coordinate is roughly represented by the stretching of the N−H bond.

After excitation the dimer becomes unstable towards dismutation (disproportionation), producing the conjugated base (A$^-$) and conjugated acid (AH$^+$) (Scheme 6). This acid/base pair is a CI S$_0$/S$_1$ providing the deactivation channel that regenerates the ground state dimer, without the need for rotation around the central C=C bond. With longer alkyl chains, either by stereochemical hindrance or entropic factors, the formation of the dimers is precluded.

Experimentally the existence of these dimers could be confirmed by transient absorption since they exhibit a strong peak at 655 nm (see Fig. SI4 in the ESI†) and emission at 673 nm. Unfortunately, these values are close to the ones observed for the monomeric species and cannot be deconvoluted from the experimental values.

*Time-resolved femtosecond transient difference absorption (fs-TA) spectra.* The time-resolved femtosecond transient difference absorption (fs-TA) spectra for NC$_1$Ind and NC$_2$Ind were recorded in the 450–800 nm range in aerated solutions with

solvents of different viscosities and dielectric constants with excitation at 550 nm. The fs-TA data for NC$_1$Ind in 2MeTHF (Table 4 and Fig. SI4†) show that the spectrum is dominated by positive broad transient absorption bands in the 560–700 nm range corresponding to the excited state absorption (ESA), accompanied by a negative feature at longer wavelength (700–800 nm range), which is attributed to stimulated emission (SE). Similar transient difference absorption bands were found for NC$_1$Ind and NC$_2$Ind in the other investigated solvents.

From Table 4 it can be seen that the decay components ($\tau_1$ and $\tau_2$) of NC$_1$Ind and NC$_2$Ind in 2MeTHF are in good agreement from time resolved measurements, mirroring the presence of the *keto* and *enol* forms. As with the ps time resolved data, fs-TA for NC$_1$Ind and NC$_2$Ind in *n*-dodecane is monoexponential. In the case of indigo carmine (indigo-5,5′-disulfonic acid disodium salt), Iwakura *et al.* showed, using a sub 5-fs laser pulse, that in methanol ultrafast single ESPT was essentially completed after 270 fs,[36–38] a study that was further recently complemented by Fleming and co-workers showing that in protic solvents intermolecular H-bonds with indigo carmine enable ESPT, generating an unstable intermediate (*enol* form) that immediately reverts back to the ground state through a CI.[33] In the present work, the CI location is almost the conjugated A$^-$/AH$^+$ pair in S$_1$, which is just 0.16 eV above S$_0$.

In our experiments, the time resolution does not allow us to observe the very short proton transfer lifetime, due to the time window limited by the instrument response function (250 fs). The fast lifetime (*keto* tautomer) could not be observed, but is evidenced (grounded in experimental work and in the TDDFT calculations) to occur in a time scale shorter than this value.

#### N,N′-Dialkyl indigo derivatives

*ps-time resolved fluorescence.* Fluorescence decays for the N,N′-dialkyl indigo derivatives collected at different emission wavelengths – along the emission band – revealed that in *n*-dodecane and MCH, with the exception of N,N′C$_1$Ind (where a single-exponential fluorescence decay is observed, Fig. 5A), all of their decays fit to a sum of two exponentials (Table SI7†). Yet, in 2MeTHF the decays are single-exponential (Fig. 5B).

As mentioned, N,N′-substituted indigo derivatives can undergo *trans–cis* photoisomerization; rotation around the central carbon–carbon bond can lead to the possible formation of conformers with different stabilities in the ground and excited states.[39] In the case of N,N′C$_2$Ind to N,N′C$_{18}$Ind, the

**Table 4** Results of the global fit analysis (lifetimes, $\tau_i$) obtained from the ultrafast time-resolved TA studies and from the ps-TCSPC technique for NC$_1$Ind and NC$_2$Ind in *n*-dodecane and 2MeTHF at T = 293 K. For indigo the same parameters are also presented in 2MeTHF for comparison

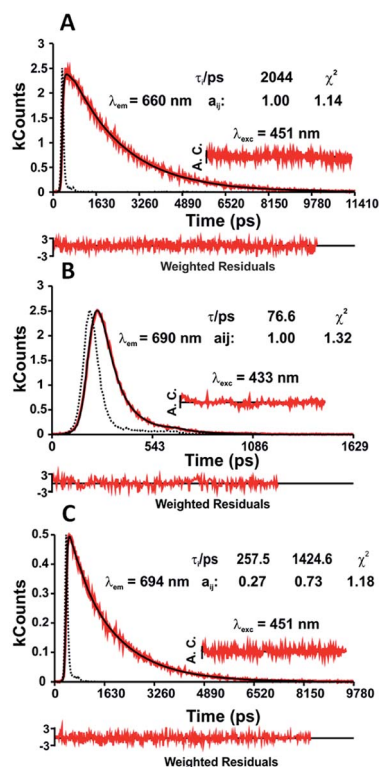| Compound | Solvent | fs-TA | | | TCSPC | | |
|---|---|---|---|---|---|---|---|
| | | $\tau_1$ (ps) | $\tau_2$ (ps) | $\tau_3$ (ps) | $\tau_1$ (ps) | $\tau_2$ (ps) | $\tau_3$ (ps) |
| **Ind**[a] | **2MeTHF** | 0.1 | 9.4 | 98.8 | | 5.9 | 128.1 |
| **NC$_1$Ind** | ***n*-Dodecane** | | 31.3 | | | 31.6 | |
| | **2MeTHF** | 9.8 | 61.0 | | 10.8 | 66.1 | |
| **NC$_2$Ind** | ***n*-Dodecane** | | 34.4 | | | 42.1 | |
| | **2MeTHF** | 10.1 | 67.0 | | 10.4 | 66.5 | |

[a] For indigo data from ref. 9.

**Fig. 5** Fluorescence decays of N,N′C$_1$Ind in MCH (A) and 2MeTHF (B) and N,N′C$_{18}$Ind in MCH (C) obtained at $T = 293$ K. The fluorescence decay times ($\tau_i$) and the associated pre-exponential factors ($a_{ij}$) are presented in the inset. For a better judgment of the quality of the fits, the weighted residuals, autocorrelation functions (ACs) and chi-squared ($\chi^2$) values are also shown. The dashed line in the decays is the pulse instrumental response.

**Table 5** Comparison of the fluorescence decay times, $\tau_i$, obtained from the ultrafast time-resolved TA studies and from the ps-TCSPC technique for N,N′C$_1$Ind and N,N′C$_2$Ind in $n$-dodecane and 2MeTHF at $T = 293$ K

| Compound | Solvent | fs-TA | | TCSPC | |
|---|---|---|---|---|---|
| | | $\tau_1$ (ps) | $\tau_2$ (ps) | $\tau_1$ (ps) | $\tau_2$ (ps) |
| **NC1Ind** | ***n*-Dodecane** | | 2387 | | 31.6 |
| | **2MeTHF** | 1.3 | 76.0 | 10.8 | 66.1 |
| **NC2Ind** | ***n*-Dodecane** | 129.9 | 1078 | 309 | 1064 |
| | **2MeTHF** | | 51.0 | | 62.4 |

Introducing a solvent field changes the relative stability of the two conformers, which deepens with the solvent polarity. In MCH the energy difference between C$_{IN}$ and C$_{OUT}$ rises to 1.3 kJ mol$^{-1}$, corresponding to a 1 : 2 relative abundance, roughly mimicking the trend expected by the analysis of the pre-exponential factors of the two decay components (Table SI7† and Fig. 5C). In THF the energy separation now rises to 3.9 kJ mol$^{-1}$, which corresponds to an 85% abundance of C$_{IN}$, making it the only detectable conformer in the time resolved decays (Fig. 5B).

*Time-resolved femtosecond transient difference absorption (fs-TA) spectra.* Time-resolved fs-TA spectra for N,N′C$_1$Ind and N,N′C$_2$Ind in $n$-dodecane and 2MeTHF were obtained with excitation at 550 nm and recorded in the 450–800 nm range. The fs-TA spectrum of N,N′C$_1$Ind in 2MeTHF (Fig. SI9†) presents positive broad transient absorption bands in the 640–750 nm range with maxima at ∼685 nm that are attributed to the excited singlet state absorption (ESA). In the 570–650 nm range, bleaching of the ground-state absorption (GSA) is observed. Similar transient difference absorption bands were found for N,N′C$_1$Ind and N,N′C$_2$Ind in the other solvent investigated. The best fit results of the characteristic fs-TA data are presented in Table 5.

The fs-TA data show that the decay components are, within experimental error, consistent with the decay time values obtained by the ps-TCSPC technique (Table 5). Moreover, the additional (in fs-TA) fast decay component observed for N,N′C$_1$Ind in 2MeTHF ($\tau_1 = 1.3$ ps) is consistent with the solvation dynamics reported for this solvent ($\tau = 0.94$ ps).[40]

observed bi-exponential fluorescence decays (Fig. 5C), together with the observed match between the excitation and absorption spectra (Fig. SI5–SI8†), show that the two components are formed in the excited state.

DFT/TDDFT calculations indicate that for N,N′C$_1$Ind only one conformer exists; yet, for longer alkyl chains two different conformers are found to be possible and, depending on the chain conformation, with differences in the energy in the S$_1$ PES that allow us to consider them as independent conformers. Fig. 6 shows the structures, here denoted as C$_{IN}$ and C$_{OUT}$. In the gas phase, C$_{IN}$ and C$_{OUT}$ are energetically separated by 0.4 kJ mol$^{-1}$ which reflects a near 50 : 50 relative abundance.
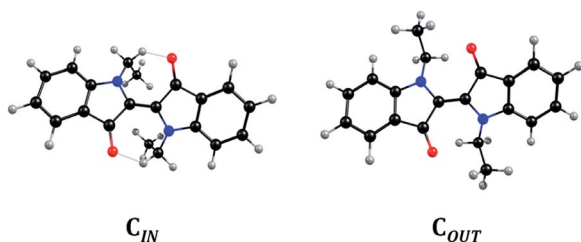
## Conclusions

A comprehensive study on the excited state behaviour of monosubstituted (NC$_n$Ind) and disubstituted (N,N′C$_n$Ind) indigo derivatives, with $n = 1$–18, has been undertaken. Several peculiarities have been found in these systems as a consequence of the solvent polarity, substitution degree and size of the alkyl chain. Excited State Proton Transfer (ESPT) is ultrafast (less than 1 ps) for NC$_{1,2}$Ind in MCH and $n$-dodecane, indicating that with short chain length monosubstituted indigo derivatives the ESPT process is ultrafast. The excited state deactivation involves a deactivation mechanism in which after the ESPT takes place in S$_1$, rotation around the central carbon–carbon bond provides access to a CI to the ground state. This is found for all NC$_n$Ind



**Fig. 6** Structures of the N,N′C$_2$Ind conformers (here denoted as C$_{IN}$ and C$_{OUT}$ in S$_1$).

derivatives in polar solvents as well as $n \geq 3$ in non-polar solvents, except for $NC_1Ind$ and $NC_2Ind$.

With the disubstituted $N,N'C_1Ind$ the decays are single-exponential, corroborating the TDDFT calculation of the presence of a major single conformer, while with the remaining $N,N'C_nInd$ ($n \geq 2$) derivatives, time-resolved studies (ps fluorescence and fs transient absorption) showed the decays to be bi-exponential, in agreement with the existence of two different conformers ($C_{IN}$ and $C_{OUT}$) in the excited state, which from TDDFT in MCH have an energetic difference of 1.3 kJ mol$^{-1}$ with a 1 : 2 relative abundance roughly mirrored by the time-resolved fluorescence data. The solvents used showed that with the $NC_nInd$ the ESPT is intramolecular, although $NC_1Ind$ and $NC_2Ind$ DFT calculations are compatible with the existence of a dimer involving the interaction between N–H and C=O groups of two different molecules.

# Experimental

## Materials

Indigo (95%) and sodium hydride (60% dispersion in mineral oil stored in a dry box) were obtained from Sigma-Aldrich. The alkyl halides (R–I) were also obtained from commercial sources (Alfa Aesar and Sigma-Aldrich). All reagents used for the synthesis of the compounds were used without further purification. For the synthetic procedures, the solvents were of commercial pro analysis (P.A.) grade. For the spectral and photophysical determinations the solvents used were of spectroscopic or equivalent grade.

## Equipment and methods

Microwave (MW)-assisted reactions were performed in a CEM Discover S-Class single-mode microwave reactor, featuring continuous temperature, pressure and microwave power monitoring.

Analytical thin-layer chromatography (TLC) was performed on Macherey-Nagel ALUGRAM Xtra silica gel plates with a $UV_{254}$ indicator. Visualization was accomplished by using an ultraviolet lamp. Silica gel column chromatography was carried out with silica gel (230–400 mesh).

Nuclear Magnetic Resonance (NMR) spectra were recorded at room temperature in $CDCl_3$ solutions on a Bruker Avance III spectrometer and a Bruker DRX-400 spectrometer, both operating at 400.13 MHz for $^1H$ and 100.61 MHz for $^{13}C$. Chemical shifts for $^1H$ and $^{13}C$ are expressed in ppm, relative to an internal standard of TMS (tetramethylsilane). Chemical shifts ($\delta$) and coupling constants ($J$) are indicated in ppm and Hz, respectively.

Gas Chromatography-Mass Spectrometry (GC-MS) analyses were performed on a Hewlett-Packard 5973 MSD spectrometer, using electron ionization (EI) (70 eV), coupled with a Hewlett-Packard Agilent 6890 chromatography system, equipped with an HP-5 MS column (30 m × 0.25 mm × 0.25 μm) and high-purity helium as a carrier gas. The initial temperature of 70 °C was increased to 250 °C at a 15 °C min$^{-1}$ rate, and held for 10 min. Then the temperature was increased to 290 °C at a 5 °C min$^{-1}$ rate and held for 2 min, giving a total run time of 32 min. The flow of the carrier gas was maintained at 1.33 mL min$^{-1}$. The injector port was set at 250 °C.

High Resolution Mass Spectrometry (HRMS) was performed on a Bruker microTOF-Focus mass spectrometer equipped with an electrospray ionization time-of-flight (ESI-TOF) source.

Absorption and fluorescence spectra were recorded on Cary 5000 UV-vis-NIR and Horiba Fluoromax 4 spectrometers, respectively. Fluorescence spectra were corrected for the wavelength response of the system.

The fluorescence quantum yields ($\phi_F$) at room temperature ($T$ = 293 K) for the $N$-alkyl indigo derivatives in the different solvents were measured using indigo ($\phi_F = 0.0023$) in DMF[9] as a standard and the equation below (eqn (2)):

$$\phi_F^{cp} = \frac{\int I(\lambda)^{cp} d\lambda}{\int I(\lambda)^{ref} d\lambda} \times \frac{n_{cp}^2}{n_{ref}^2} \times \phi_F^{ref} \qquad (2)$$

where $\int I(\lambda)^{cp} d\lambda$ is the integrated area under the emission spectra of the compound (cp) solutions and $\int I(\lambda)^{ref} d\lambda$ is for the reference (ref) solution, $n_{cp}^2$ and $n_{ref}^2$ are the refractive indices of the solvents in which the compounds and the reference were respectively dissolved and $\phi_F^{ref}$ is the fluorescence quantum yield of the standard. The fluorescence quantum yields ($\phi_F$) at $T$ = 293 K for $N,N'$-dialkyl indigo derivatives in the different solvents were also obtained by the comparative method (eqn (2)) using the fluorescence quantum yields ($\phi_F$) of $N$-alkyl indigo derivatives in the different solvents as standards.

Fluorescence decays were measured using a home-built picosecond time-correlated single photon counting (ps-TCSPC) apparatus described elsewhere.[41] The excitation source consists of a tunable picosecond Spectra-Physics mode-lock Tsunami laser (Ti:sapphire) model 3950 (80 MHz repetition rate, tuning range 700–1000 nm), pumped by a 532 nm continuous wave Spectra-Physics Millennia Pro-10s laser. The excitation wavelength ($\lambda_{exc}$ = 433 nm) was obtained with a Spectra-Physics harmonic generator, model GWU-23PS. Alternatively, a Pico-Quant PicoLED model LDH-P-C-450B with wavelength $\lambda_{exc}$ = 451 nm was also used as an excitation source. To eliminate stray light from the light source, an RG530 filter was placed between the sample holder and the emission monochromator. The fluorescence decay curves were deconvoluted using the experimental instrument response function signal collected with a scattering solution (aqueous Ludox solution). The deconvolution procedure was performed using the modulation function method, as implemented by G. Striker in the SAND program, and previously reported in the literature.[42]

The experimental setup for the ultrafast spectroscopic and kinetics measurements consisted of a broadband (350–1600 nm) HELIOS pump–probe femtosecond transient absorption spectrometer from Ultrafast Systems, pumped by an amplified femtosecond Spectra-Physics Solstice-100F laser (800 nm central wavelength, 128 fs pulse width and 1 kHz repetition rate) and coupled with a Spectra-Physics TOPAS Prime F optical parametric amplifier (195–22 000 nm tuning range). The probe light in the

UV range was generated by passing a small portion of the 800 nm light from the Solstice-100F laser through a computerized optical delay (with a time window of up to 8 ns) and then focusing it on a vertical translating $CaF_2$ crystal to generate a white-light continuum (350–750 nm). All the measurements were obtained in a 2 mm quartz cuvette, with absorptions of $\sim$0.3 at the pump excitation wavelength. To avoid photodegradation, the solutions were stirred during the experiments or kept in movement with a frequency lower than that of the laser using a motorized translating sample holder. Background signals from impurities or unwanted coherent effects were ruled out by scans of the neat solvent. The spectral chirp of the data was corrected using the Surface Xplorer PRO program from Ultrafast Systems. Global analysis of the data (using a sequential model) was performed using Glotaran software.[43]

### Computational details

All theoretical calculations were of the density functional theory (DFT) type, carried out using GAMESS-US version R3.[44] A range corrected LC-BPBE ($\omega = 0.2$ au$^{-1}$) functional, as implemented in GAMESS-US,[45] was used in both ground- and excited-state calculations. TDDFT calculations, with similar functionals, were used to probe the excited-state potential energy surface (PES). The solvent was included using the polarizable continuum model with the solvation model density to add corrections for cavitation, dispersion, and solvent structure. In the TDDFT calculation of FC (Franck–Condon) excitations the dielectric constant of the solvent was split into a "bulk" component and a fast component, which is essentially the square of the refractive index.[46] Under "adiabatic" conditions only the static dielectric constant is used. A 6-31G** basis set was used in either DFT or TDDFT calculations. Fast probing of $S_n$ Potential Energy Surfaces (PESs), for location of critical points, was carried out using SBKJC ECPs (Stevens–Basch–Krauss–Jasien–Cundari Effective Core Potentials for non-valence electrons with a split-31G for valence electrons),[47–49] although when photophysical properties were evaluated the preliminary results were recalculated using the more extensive 6-31G** basis set.

Probing of the potential energy surface to locate the conical intersection (CI) was based on the anchor points defined by the *trans* and *cis* $S_1$ optimized structures connected to the apex of the isomerization barrier by an IRC (internal reaction coordinate). By using Hessians along this IRC path we identified possible reactive normal modes, parallel to the IRC, that could correspond to the branching space of the CI and, along them, minimized $\Delta E = E(S_1) - E(S_0)$ until a predefined threshold of 0.05 eV (or less) was observed.[50,51]

## Conflicts of interest

The authors declare that there are no conflicts to declare.

## Acknowledgements

## References

1 N. Gaboriaud-Kolar, S. Nam and A.-L. Skaltsounis, *Progress In The Chemistry of Organic Natural Products*, Springer, 2014.

2 J. S. Seixas de Melo, in *Photochemistry: Volume 45*, The Royal Society of Chemistry, 2018, vol. 45, pp. 68–100.

3 J. S. Seixas de Melo, in *Photochemistry*, ed. A. Albini and S. Prodi, RSC, London, 2020, vol. 47, pp. 196–216.

4 C. Fang and B. Durbeej, *J. Phys. Chem. A*, 2019, **123**, 8485–8495.

5 J. Pina, D. Sarmento, M. Accoto, P. L. Gentili, L. Vaccaro, A. Galvão and J. S. Seixas de Melo, *J. Phys. Chem. B*, 2017, **121**, 2308–2318.

6 A. L. Costa, A. C. Gomes, M. Pillinger, I. S. Gonçalves and J. S. Seixas de Melo, *Chem.–Eur. J.*, 2015, **21**, 12069–12078.

7 G. Cui and W. Thiel, *Phys. Chem. Chem. Phys.*, 2012, **14**, 12378–12384.

8 R. Rondão, J. S. Seixas de Melo, F. A. Schaberle and G. Voss, *Phys. Chem. Chem. Phys.*, 2012, **14**, 1778–1783.

9 J. S. Seixas de Melo, R. Rondão, H. D. Burrows, M. J. Melo, S. Navaratnam, R. Edge and G. Voss, *ChemPhysChem*, 2006, **7**, 2303–2311.

10 S. Yamazaki, A. L. Sobolewski and W. Domcke, *Phys. Chem. Chem. Phys.*, 2011, **13**, 1618–1628.

11 J. S. Seixas de Melo, R. Rondão, H. D. Burrows, M. J. Melo, S. Navaratnam, R. Edge and G. Voss, *J. Phys. Chem. A*, 2006, **110**, 13653–13661.

12 C. Ma, H. Li, Y. Yang, D. Li and Y. Liu, *Chem. Phys. Lett.*, 2015, **638**, 72–77.

13 D. Jacquemin, J. Preat, V. Wathelet, M. Fontaine and E. A. Perpète, *J. Am. Chem. Soc.*, 2006, **128**, 2072–2083.

14 C.-Y. Huang, A. Bonasera, L. Hristov, Y. Garmshausen, B. M. Schmidt, D. Jacquemin and S. Hecht, *J. Am. Chem. Soc.*, 2017, **139**, 15205–15211.

15 H. Nakagawa, A. Matsumoto, A. Daicho, Y. Ozaki, C. Ota and Y. Nagasawa, *J. Photochem. Photobiol., A*, 2017, **358**, 308–314.

16 E. C. Nicholls-Allison, G. Nawn, B. O. Patrick and R. G. Hicks, *Chem. Commun.*, 2015, **51**, 12482–12485.

17 J. Pouliquen, V. Wintgens, V. Toscano and J. Kossanyi, *Dyes Pigm.*, 1985, **6**, 163–175.

18 Y. Omote, S. Imada, R. Matsuzaki, K. Fujiki, T. Nishio and C. Kashima, *Bull. Chem. Soc. Jpn.*, 1979, **52**, 3397–3399.

19 J. Blanc and D. L. Ross, *J. Phys. Chem.*, 1968, **72**, 2817–2824.

20 J. Weinstein and G. M. Wyman, *J. Am. Chem. Soc.*, 1956, **78**, 4007–4010.

21 D. Jacquemin, J. Preat, V. Wathelet and E. A. Perpète, *J. Chem. Phys.*, 2006, **124**, 0741041–07410412.

22 E. A. Perpète, J. Preat, J.-M. André and D. Jacquemin, *J. Phys. Chem. A*, 2006, **110**, 5629–5635.

23 G. M. Wyman and B. M. Zarnegar, *J. Phys. Chem.*, 1973, **77**, 1204–1207.

24 G. M. Wyman and B. M. Zarnegar, *J. Phys. Chem.*, 1973, **77**, 831–837.

25 C. Giuliano, L. Hess and J. Margerum, *J. Am. Chem. Soc.*, 1968, **90**, 587–594.

26 J.-I. Setsune, *J. Synth. Org. Chem., Jpn.*, 1988, 681–692.

27 P. Brandão, D. Pinheiro, J. S. Seixas de Melo and M. Pineiro, *Dyes Pigm.*, 2020, **173**, 107935.

28 P. Zhou, M. R. Hoffmann, K. Han and G. He, *J. Phys. Chem. B*, 2015, **119**, 2125–2131.

29 G.-Y. Li, G.-J. Zhao, Y.-H. Liu, K.-L. Han and G.-Z. He, *J. Comput. Chem.*, 2010, **31**, 1759–1765.

30 S. Chai, G.-J. Zhao, P. Song, S.-Q. Yang, J.-Y. Liu and K.-L. Han, *Phys. Chem. Chem. Phys.*, 2009, **11**, 4385–4390.

31 W. R. Laws and L. Brand, *J. Phys. Chem.*, 1979, **83**, 795–802.

32 M. J. Melo, J. L. Ferreira, A. J. Parola and J. S. Seixas de Melo, *Applied Photochemistry:When Light Meets Molecules*, Springer International Publishing, Switzerland, 2016.

33 P. P. Roy, J. Shee, E. A. Arsenault, Y. Yoneda, K. Feuling, M. Head-Gordon and G. R. Fleming, *J. Phys. Chem. Lett.*, 2020, **11**, 4156–4162.

34 Y. Nagasawa, R. Taguri, H. Matsuda, M. Murakami, M. Ohama, T. Okada and H. Miyasaka, *Phys. Chem. Chem. Phys.*, 2004, **6**, 5370–5378.

35 P. Su and H. Li, *J. Chem. Phys.*, 2009, **131**, 014102.

36 I. Iwakura, A. Yabushita and T. Kobayashi, *Bull. Chem. Soc. Jpn.*, 2011, **84**, 164–171.

37 I. Iwakura, A. Yabushita and T. Kobayashi, *Chem. Phys. Lett.*, 2010, **484**, 354–357.

38 I. Iwakura, A. Yabushita and T. Kobayashi, *Chem. Lett.*, 2009, **38**, 1020–1021.

39 D. C. Nobre, C. Cunha, A. Porciello, F. Valentini, A. Marrocchi, L. Vaccaro, A. M. Galvão and J. S. Seixas de Melo, *Dyes Pigm.*, 2020, **176**, 108197.

40 M. L. Horng, J. A. Gardecki, A. Papazyan and M. Maroncelli, *J. Phys. Chem.*, 1995, **99**, 17311–17337.

41 J. Pina, J. S. Seixas de Melo, H. D. Burrows, A. L. Maçanita, F. Galbrecht, T. Bünnagel and U. Scherf, *Macromolecules*, 2009, **42**, 1710–1719.

42 G. Striker, V. Subramaniam, C. A. M. Seidel and A. Volkmer, *J. Phys. Chem. B*, 1999, **103**, 8612–8617.

43 J. J. Snellenburg, S. Laptenok, R. Seger, K. M. Mullen and I. H. M. Van Stokkum, *J. Stat. Softw.*, 2012, **49**, 1–22.

44 M. W. Schmidt, K. K. Baldridge, J. A. Boatz, S. T. Elbert, M. S. Gordon, J. H. Jensen, S. Koseki, N. Matsunaga, K. A. Nguyen, S. Su, T. L. Windus, M. Dupuis and J. A. Montgomery Jr, *J. Comput. Chem.*, 1993, **14**, 1347–1363.

45 T. Yanai, D. P. Tew and N. C. Handy, *Chem. Phys. Lett.*, 2004, **393**, 51–57.

46 M. Cossi and V. Barone, *J. Chem. Phys.*, 2001, **115**, 4708–4717.

47 T. R. Cundari and W. J. Stevens, *J. Chem. Phys.*, 1993, **98**, 5555–5565.

48 W. J. Stevens, M. Krauss, H. Basch and P. G. Jasien, *Can. J. Chem.*, 1992, **70**, 612–630.

49 W. J. Stevens, H. Basch and M. Krauss, *J. Chem. Phys.*, 1984, **81**, 6026–6033.

50 A. M. Galvão, *J. Photochem. Photobiol., A*, 2014, **289**, 66–72.

51 B. Dick, Y. Haas and S. Zilberg, *Chem. Phys.*, 2008, **347**, 65–77.